THE JOURNAL OF PHYSICAL CHEMISTRY B

Article

pubs.acs.org/JPCB

Force-Induced Unzipping Transitions in an Athermal Crowded Environment

David L. Pincus and D. Thirumalai*

Institute for Physical Science and Technology, University of Maryland, College Park, Maryland 20742, United States

ABSTRACT: Using theoretical arguments and extensive Monte Carlo (MC) simulations of a coarse-grained three-dimensional off-lattice model of a β-hairpin, we demonstrate that the equilibrium critical force, F_c, needed to unfold the biopolymer increases nonlinearly with increasing volume fraction occupied by the spherical macromolecular crowding agent. Both scaling arguments and MC simulations show that the critical force increases as $F_c \approx \varphi_c^{\alpha}$. The exponent α is linked to the Flory exponent relating the size of the unfolded state of the biopolymer and the number of amino acids. The predicted power law dependence is confirmed in simulations of the dependence of the isothermal extensibility and the fraction of native contacts on φ_c. We also show using MC simulations that F_c is linearly dependent on the average osmotic pressure (P) exerted by the crowding agents on the β-hairpin. The highly significant linear correlation coefficient of 0.99657 between F_c and P makes it straightforward to predict the dependence of the critical force on the density of crowders. Our predictions are amenable to experimental verification using laser optical tweezers.

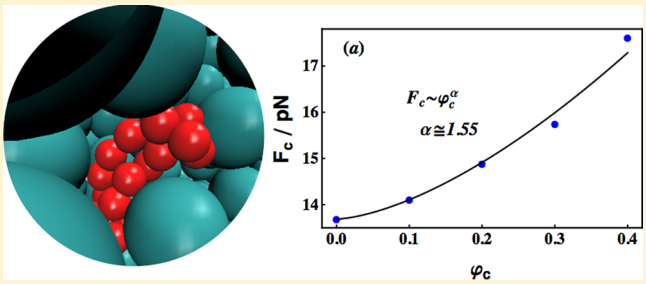

INTRODUCTION

The study of the protein folding problem was galvanized by using concepts from the physics of disordered systems. Using a coarse-grained description of folding, expressed in terms of an uncorrelated distribution of energies of protein conformations corresponding to the values at local minima in a multidimensional energy landscape, Bryngelson and Wolynes[1,2] mapped the problem of equilibrium statistical mechanics of protein folding to a random energy model in which the native state plays a special role. These influential works and subsequent studies[3] showed that most naturally evolved sequences are foldable, which means that they reach the stable native state on biologically relevant time scales. In this picture, foldable sequences are characterized by large differences in the environmental-dependent folding temperature (T_f) and the glass transition temperature (T_g) at which the kinetics becomes so sluggish that the folded state is inaccessible on biologically relevant time scales. Related ideas rooted in polymer physics further showed that the interplay of T_f, and the equilibrium collapse temperature (T_θ)[4] could be used to not only fully characterize the phase diagram of generic protein sequences but also determine their foldability, a prediction that has been experimentally validated very recently.[5] In the intervening years, an impressively large number of important theoretical and experimental works (for a recent collection, see ref 6 and references cited therein) on a variety of seemingly unrelated problems associated with protein folding have appeared, thus greatly expanding the scope and utility of concepts from statistical mechanics and polymer physics. Through these developments, an expansive view of protein folding and its role in biophysics has emerged[7] with current applications ranging from assisted folding[8−11] to describing the functions of molecular motors[12−16] using models originally devised to understand protein folding kinetics.

A particularly important problem that has benefited from the focus on protein folding is the role molecular crowding plays in modulating the thermodynamics and kinetics of folding of proteins[17] and RNA[18−20] although its importance was recognized long ago.[21] It is now widely appreciated that the cytosol is a crowded heterogeneous medium containing a variety of macromolecules such as ribosomes, lipids, and RNA. As a result, folding, diffusion, and other biological processes in such an environment could be different from what transpires under infinite dilution conditions. The effects of macromolecular crowding on the stability of synthetic as well as biopolymers have been extensively investigated[17,19−33] because of the potential relevance for folding under cellular conditions. In general, several interaction energy and length scales determine whether crowding agents stabilize, have negligible effect, or even destabilize the folded states of proteins.[29] As a result a number of scenarios can emerge depending on the nature of crowding agents, and the choice of proteins. The simplest scenario arises when both the crowder−crowder and crowder−protein interactions are dominated by excluded volume. Although this situation may not accurately characterize even *in vitro* experiments, it has the advantage that folding in this situation can be described using a combination of scaling arguments and simulations.[29] Nonspecific athermal crowders

Special Issue: Peter G. Wolynes Festschrift

Received: March 25, 2013
Revised: June 18, 2013
Published: June 21, 2013

 © 2013 American Chemical Society dx.doi.org/10.1021/jp402922q | *J. Phys. Chem. B* 2013, 117, 13107−13114

(only the excluded volume interactions between the crowders and the crowder and the protein are relevant) tend to shift the folded ⇌ unfolded (or equivalently the zipped ⇌ unzipped) equilibrium of a biopolymer toward the folded state by the entropic stabilization theory (EST), because this maximizes the free-volume available (and hence entropy) to the crowding agents. This simple theory is based on the elegant concept of depletion interaction,[34−37] which posits that the crowding particles decrease the entropy of the unfolded state to a greater extent than the folded state, thus differentially stabilizing the ordered structure.[29]

The EST can be validated by measuring the dependence of the melting temperature on the volume fraction (φ_c) of the crowding particles. If EST is valid then $\Delta T_m(\varphi_c) = T_m(\varphi_c) - T_m(0)$ should increase. Indeed, absence of any change in $\Delta T_m(\varphi_c)$ indicates that enthalpic effects play an important role. Another way to quantify the extent of stabilization is to ask what critical force (F_c) would be necessary to unfold a biopolymer at a given volume fraction (φ_c) of the crowding agents. In this paper, we study the simple case of unzipping a polypeptide chain that forms a β-hairpin by applying mechanical force as a function of volume fractions of monodisperse spherical crowding particles. The study of the zipping/unzipping of biopolymers has a rich history[38−49] and has even formed the basis of assessing folding mechanisms of proteins.[50]

Surprisingly, there have been very few experimental[51,52] or theoretical studies[18] investigating the effect of mechanical force on proteins in a crowded environment. The experimental studies have argued that F_c increases linearly with φ_c, whereas the theoretical arguments[18] predict a nonlinear dependence, which was shown to provide a good fit to the experimental data. In this paper, we argue that the unzipping of a biopolymer under *constant* tension could be consistent with linear dependence only for small φ_c. At higher volume fractions, F_c does increase nonlinearly with φ_c. The increase in F_c, relative to its value at $\varphi_c = 0$, linked to crowding-induced stability, arises because of a depletion of the crowding particles from the proximity of proteins. This, in turn, results in the crowding agents exerting an osmotic pressure on the biopolymer. Unzipping the biopolymer requires that the imposed tension perform work against this osmotic pressure. Thus, it is natural to assume that F_c should be linearly dependent on the average pressure (P) associated with crowding particles modeled as hard spheres. We have verified this relation using extensive Monte Carlo simulations, and we present a simple method for determining F_c at an arbitrary φ_c once the linear dependence of F_c on P is known.

METHODS

Model. In order to explore the effects of crowding on the unzipping of a biopolymer, we chose the 16 residue sequence that forms a β-hairpin structure and had been previously used to illustrate the effects of confinement on protein folding.[48] The structure corresponds to the C-terminal β-hairpin of protein G (PDB accession ID 1GB1), a model system that has been extensively studied using computations[53−59] following an initial pioneering experimental study.[50]

In our simulations, we used a coarse-grained representation of the polypeptide chain. We modeled the hairpin as a collection of $N_p = 16$ spheres of diameter $\sigma_p = 0.38$ nm (each representing a residue) with configuration $\{\mathbf{r}_i\}_{i=1}^{N_p}$, and crowders as a monodisperse collection of N_c spheres of diameter $\sigma_c = 1.0$ nm with configuration $\{\mathbf{R}_l\}_{l=1}^{N_c}$. The Hamiltonian depended on both the positions of the crowders and the conformations of the polypeptide chain:

$$\mathcal{H}(\{\mathbf{r}_i\}, \{\mathbf{R}_l\}) \equiv \mathcal{H}_{cc}(\{\mathbf{R}_l\}) + \mathcal{H}_{pp}(\{\mathbf{r}_i\}) + \mathcal{H}_{pc}(\{\mathbf{r}_i\}, \{\mathbf{R}_l\}) + \mathcal{H}_{bond}(\{\mathbf{r}_i\}) + \mathcal{H}_{coop}(\{\mathbf{r}_i\}) \quad (1)$$

The first three terms on the right-hand side (rhs) of eq 1 accounted for nonbonded crowder−crowder (cc), protein−protein (pp), and protein−crowder (pc) interactions, respectively. The penultimate term on the rhs of eq 1 ($\mathcal{H}_{bond}(\{\mathbf{r}_i\})$) was used to enforce chain connectivity, while the final term on the rhs of eq 1 ($\mathcal{H}_{coop}(\{\mathbf{r}_i\})$) was used to ensure that the hairpin underwent a cooperative unzipping transition under tension. The interactions between the crowding particles were taken to be

$$\mathcal{H}_{cc}(\{\mathbf{R}_l\}) = \sum_{J>l} \upsilon_{cc}(|\mathbf{R}_l - \mathbf{R}_J|) \quad (2)$$

where

$$\upsilon_{cc}(r) = \begin{cases} \infty & (r \le \sigma_c) \\ 0 & (r > \sigma_c) \end{cases} \quad (3)$$

Similarly, we used hard-sphere potentials to model the interactions between the crowders and the polypeptide (pc):

$$\mathcal{H}_{pc}(\{\mathbf{r}_i\}, \{\mathbf{R}_l\}) = \sum_{i,l} \upsilon_{pc}(|\mathbf{R}_l - \mathbf{r}_i|) \quad (4)$$

where

$$\upsilon_{pc}(r) = \begin{cases} \infty & (r \le (\sigma_p + \sigma_c)/2) \\ 0 & (r > (\sigma_p + \sigma_c)/2) \end{cases} \quad (5)$$

The term $\mathcal{H}_{pp}(\{\mathbf{r}_i\},\{\mathbf{r}_i^0\})$ in eq 1 was decomposed into native (N) and non-native (NN) contributions by partitioning the set of residue−residue distances into those that were less than a cutoff ($R_{cut} = 0.8$ nm) in the crystal structure and those greater than R_{cut} (i.e., $\{\{|\mathbf{r}_i - \mathbf{r}_j|\} \equiv \{\mathbf{r}_{ij}\}=\{\mathbf{r}_{ij}:|\mathbf{r}_i^0 - \mathbf{r}_j^0| \le R_{cut}\}\cup\{\mathbf{r}_{ij}:|\mathbf{r}_i^0 - \mathbf{r}_j^0| > R_{cut}\}$). Letting $\eta = \{\mathbf{r}_{ij}:|\mathbf{r}_i^0 - \mathbf{r}_j^0| \le R_{cut}\}$ and $\vartheta = \{\mathbf{r}_{ij}:|\mathbf{r}_i^0 - \mathbf{r}_j^0| > R_{cut}\}$, we write

$$\mathcal{H}_{pp}(\{\mathbf{r}_i\}, \{\mathbf{r}_i^0\}) = \mathcal{H}_{pp}^{N}(\eta) + \mathcal{H}_{pp}^{NN}(\vartheta) \quad (6)$$

$$\mathcal{H}_{pp}^{N}(\eta) = \sum_{d\in\eta} \upsilon_{pp}^{N}(d) \quad (7)$$

with

$$\upsilon_{pp}^{N}(d) = \begin{cases} \infty & (d/d^0 < 0.8) \\ -\epsilon & (0.8 \le d/d^0 < 1.2) \\ 0 & (d/d^0 > 1.2) \end{cases} \quad (8)$$

where d^0 is the value of d in the crystal structure.

Similarly,

$$\mathcal{H}_{pp}^{NN}(\vartheta) = \sum_{d\in\vartheta} \upsilon_{pp}^{NN}(d) \quad (9)$$

where

dx.doi.org/10.1021/jp402922q | J. Phys. Chem. B 2013, 117, 13107−13114

$$v_{pp}^{NN}(d) = \begin{cases} \infty & (d \le \sigma_p) \\ 0 & (d > \sigma_p) \end{cases} \tag{10}$$

Chain connectivity was enforced with a sum of box-like terms:

$$\mathcal{H}_{bond}(\{\mathbf{r}_i\}) = \sum_{i<N_p} v_{bond}(|\mathbf{r}_{i+1} - \mathbf{r}_i|) \tag{11}$$

where

$$v_{bond}(r) = \begin{cases} \infty & r/r_b^0 < 0.8 \\ 0 & 0.8 \le r/r_b^0 \le 1.2 \\ \infty & r/r_b^0 > 1.2 \end{cases} \tag{12}$$

and r_b^0 is an ideal $C_\alpha - C_\alpha$ "bonding" distance of 0.38 nm.

The cooperativity term ($\mathcal{H}_{coop}(\{\mathbf{r}_i\})$) is a coarse-grained representation of hydrogen-bonding type interactions and has a nearest-neighbor Ising-like character,

$$\mathcal{H}_{coop}(\{\mathbf{r}_i\}) = -J \sum_{l=2}^{ncoop} \Theta(d_l^0 - d_l)\Theta(d_{l-1}^0 - d_{l-1}) \tag{13}$$

where $J = \epsilon/5$, $\Theta(x)$ is a Heaviside function, and d_l (d_l^0) is the distance (PDB distance) separating a pair of complementary residues in the strand (l and $l-1$ denote nearest neighbor pairs). There were ncoop = 7 pairs of complementary residues in the strand with PDB numbering: {{41,56},{42,55},{43,54},{44,53},{45,52},{46,51},{47,50}} (see Figure 1 for the numbering of the residues as well as the seqence). Note that not all of these residue pairs are hydrogen bonded in the native hairpin. In general, strand pairs exist as parts of larger β-sheets and make some hydrogen bonds between the strands of the pair as well as some hydrogen bonds with other strands of the sheet. The coarse-grained nature of eq 13 renders the model sufficiently general to ensure transferability to models of RNA or DNA hairpins. Under such circumstances, eq 13 would mimic the stacking interactions, which are known to stabilize nucleic acids.

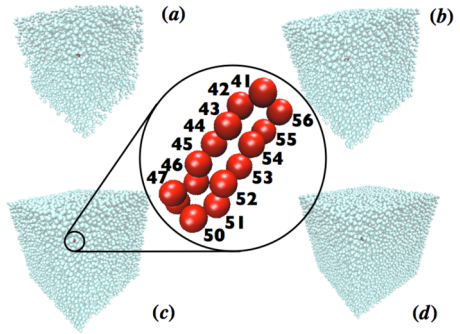

Figure 1. Snapshots of the simulated system in the absence of mechanical force: (a) $\varphi_c = 0.1$ ($N_c = 5000$); (b) $\varphi_c = 0.2$ ($N_c = 10000$); (c) $\varphi_c = 0.3$ ($N_c = 15000$); (d) $\varphi_c = 0.4$ ($N_c = 20000$). The hairpin corresponds to the small dark spot at the center of each of the boxes. The center of the figure shows a blowup of the region adjacent to the hairpin. The purpose of showing the four snapshots is to illustrate that the biopolymer is jammed in a sea of crowding particles. The blowup in the center shows structure of the β-hairpin along with the sequence numbering of the 16 residues.

Simulation Methods. We used a standard Metropolis algorithm to simulate the model described by eq 1 and to obtain thermodynamic quantities of interest. Crowder trial moves were attempted in a "single-spin flip" manner and consisted of random repositioning of a crowder through the generation of three independent and uniformly distributed random variables (rv's) on the interval $[-L/2,L/2]$, where L = 29.7 nm is the length of a side of the cubic simulation box.

The position of residue 1 of the hairpin was held fixed at the origin throughout all simulations (i.e., $\mathbf{r}_1(t) = \mathbf{0}\ \forall t$). The remaining $N_p - 1$ residue trial moves were randomly selected from a set of two possibilities. One type of move corresponded to that used by Baumgärtner and Binder[60] for simulating a freely jointed chain; a random angle γ was chosen from a uniform distribution on $[0,2\pi)$ and an attempt was made to displace residue i by γ radians along the circle perpendicular to the line connecting residues $i-1$ and $i+1$. For the residue at the free-end of the chain two random angles (β,γ) were chosen, and an attempt was made to move the residue to a new point on the sphere centered at residue $N_p - 1$. The second type of move corresponded to a random change in the bond length connecting residue i to residue $i-1$ ($i = 2, 3, ..., N_p$); a uniform rv, $\mathcal{N}$, on (0.8,1.2) was generated, and an attempt was made to map $\mathbf{r}_i \mapsto (\mathbf{r}_i - \mathbf{r}_{i-1})\mathcal{N} + \mathbf{r}_{i-1}$. A trial move from $\mu \to \nu$ was accepted with probability ($A(\mu \to \nu)$):

$$A(\mu \to \nu) = \begin{cases} e^{-(\mathcal{H}_\nu - \mathcal{H}_\mu)/(k_B T)} e^{(1/k_B T)F(z_\nu - z_\mu)} & (\mathcal{H}_\nu - \mathcal{H}_\mu) \\ & \quad - F(z_\nu - z_\mu) > 0 \\ 1 & \text{otherwise} \end{cases} \tag{14}$$

where T is the temperature, k_B is Boltzmann's constant, $\mathcal{H}_\nu$ and $\mathcal{H}_\mu$ are as above, F is the constant tension applied to the polymer, and z_ν and z_μ are the extension in state ν and μ, respectively, of the polymer in the direction of the applied force.

Data Collection. Time, measured in Monte Carlo steps (MCS), corresponded to the attempted displacement of ($N_c + N_p - 1$) particles, since one end of the chain was always held fixed to the origin. Data from a trajectory were collected every 1000 MCS. Figure 2 reveals that this is significantly longer than

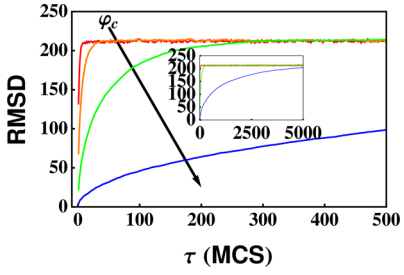

Figure 2. Root mean square deviation (rmsd) of the crowding agents from an equilibrated initial state as a function of time (τ, measured in Monte Carlo steps per free particle (MCS)) for trajectories at $\varphi_c = 0.1$ (blue), $\varphi_c = 0.2$ (green), $\varphi_c = 0.3$ (orange), and $\varphi_c = 0.4$ (red). Note that crowder trial moves are reasonably successful for $\varphi_c \le 0.3$, which implies that the allowed conformations are ergodically sampled. The acceptance ratio for such trial moves is significantly reduced at $\varphi_c = 0.4$ although the errors in the results are small as indicated by consistency between different measures. The sampling interval used for collecting the data presented in all figures below was 1000 MCS.

dx.doi.org/10.1021/jp402922q | J. Phys. Chem. B 2013, 117, 13107−13114

the time required for the RMSD of the crowding agents from an equilibrated initial state to plateau at all volume fractions except $\varphi_c = 0.4$. Even at $\varphi_c = 0.4$, the RMSD has increased substantially after 1000 MCS. We used 0, 5000, 10000, 15000, and 20000 crowders to simulate crowder volume fractions of 0.0, 0.1, 0.2, 0.3, and 0.4, respectively. For each φ_c, data was collected at tensions between 0 pN and 40 pN at 1 pN intervals. Snapshots of simulations at each of the nonzero φ_c and in the absence of tension are illustrated in Figure 1. Data at each force and each φ_c was collected from multiple trajectories starting from previously equilibrated configurations (in turn based on trajectories initiated from random initial crowder configurations at both high- and low-force hairpin configurations).

RESULTS

Radial Distribution between Crowders and the Hairpin. Figure 3 is a plot of the radial distribution ($g(r)$) of crowders about the center of mass of the hairpin versus distance (r) (i.e., $g(r) = V/[N_c]\langle\sum_i \delta(\mathbf{r} - (\mathbf{R}_i - \mathbf{r}_{cm}))\rangle$). The maxima in these plots correspond to the average diameter of the region to which the hairpin finds itself confined (D). Interestingly, the plots illustrate that the average size of the region is inversely proportional to the crowder density (i.e., $D \approx \varphi_c^{-1}$). This suggests that, perhaps, the region in which the hairpin on average is localized is aspherical.[61] If the region were spherical, we would expect that $D \approx \varphi_c^{-1/3}$.

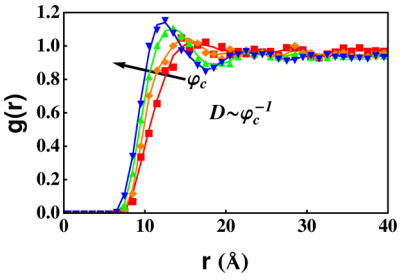

Figure 3. Radial distribution function ($g(r)$) of the crowders about the center of mass of the hairpin at various volume fractions and at $F = 0$ pN. Red squares, orange diamonds, green upward triangles, and blue downward triangles, respectively, correspond to $\varphi_c = 0.1$, 0.2, 0.3, and 0.4. The maxima in $g(r)$ lie at $r = 15.5$, 14.5, 13.5, and 12.5 Å, respectively. This suggests that the size of the region to which the hairpin is confined (D) is inversely proportional to φ_c, implying that this region is aspherical. The symbols represent raw data; curves correspond to smoothing using eq 6.48 of Allen and Tildesley.[66]

The observation that $D \approx \varphi_c^{-1}$ in conjunction with an approximate mapping between crowding and confinement could be used to obtain the expected scaling of the dependence of the critical force required to the unfold the β-hairpin, F_c, on φ_c. Because the confining region is described by a single length, D, the EST can be used to identify the enhancement in the stability of the ordered state with the loss in entropy of the unfolded state upon confinement. A similar scaling approach, using concepts developed in the context of polymer physics, has been used to study confinement effects on biopolymers.[48,62−64] Using this inherently mean-field argument, we expect

$$F_c \approx T\Delta S/\Delta x_u^{\ddagger} \approx (R_g/D)^{1/\nu}\frac{k_B T}{\Delta x_u^{\ddagger}} \approx A\varphi_c^{1/\nu} \quad (15)$$

In the above equation, $T\Delta S$ is the penalty for confining the polypeptide chain with dimension R_g in a region with size D, $\Delta x_u^{\ddagger}$ is the minimum extension needed to unfold the protein, and ν is the Flory exponent. Because $D \approx \varphi_c^{-1}$, we expect that $F_c \approx \varphi_c^{1/\nu} \approx \varphi_c^{5/3}$ assuming that $\nu \approx 0.6$. If $D \approx \varphi_c^{-1/3}$, as would be the case if the unfolded state were spherical, then it follows that $F_c \approx \varphi_c^{5/9}$, a result that we derived previously[18] to analyze the experimental data on forced unfolding of ubiquitin.

Numerical Evidence for Equation 15. Plots of the average extension of the hairpin ($\langle z\rangle$) versus applied tension (F) presented in Figure 4a show that the $\langle z\rangle$ decreases monotonically with φ_c at moderate values of F. This implies that crowding in essence decreases $\langle z\rangle$ because the entropic penalty to stretch a protein in a crowded environment is far too large. In other words, the probability of finding a region free of crowders decreases exponentially as the extension increases, which explains the observed results in Figure 4a. The isothermal extensibility ($\chi \equiv \partial\langle z\rangle/\partial F$) plots in Figure 4b reveal that F_c (i.e., the value of F at which χ is a maximum) increases monotonically with increasing φ_c. A plot of F_c versus φ_c (Figure 5a) subsequently revealed that the power-law dependence of F_c on φ_c is characterized by an exponent $\alpha \cong 1.6$, which is in accord with the scaling predictions in eq 15. Data collapse of χ based on a scaling function $X((F - F_c)/F_c)$ that is independent of N_c revealed that $\chi \approx (1 - AN_c^{d_\chi})$, where $d_\chi \cong 1.43$ and $A \cong 1.7 \times 10^{-7}$. This shows that the effects of crowding and force can be separated, which to some extent justifies the scaling theory predictions. Thus, when measured in terms of the reduced distance to the critical force, the primary effect of the crowders is to decrease the extensibility of the chain.

We can also obtain the dependence of F_c on φ_c using the F-dependent changes in an order parameter that characterizes the

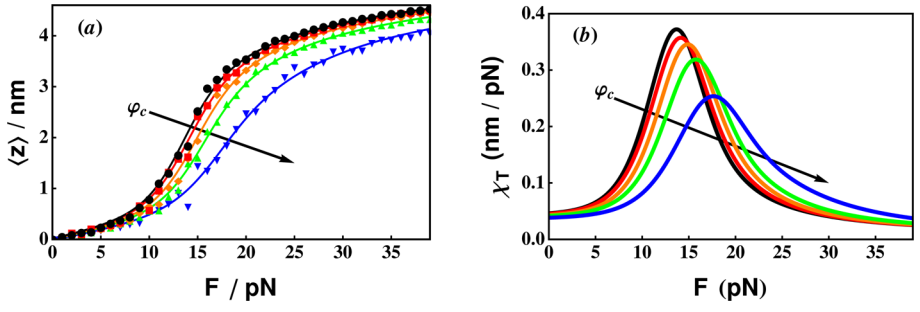

Figure 4. Plot of (a) average extension ($\langle z\rangle$) as a function of force (F) and (b) isothermal extensibility ($\chi \equiv \partial\langle z\rangle/\partial F|_T$) versus force ($F$). Black, red, orange, green, and blue curves, respectively, correspond to volume fractions (φ_c) of 0, 0.1, 0.2, 0.3, and 0.4. All curves were calculated using the multiple histogram reweighting method; symbols in plot a correspond to unreweighted data.

dx.doi.org/10.1021/jp402922q | J. Phys. Chem. B 2013, 117, 13107−13114

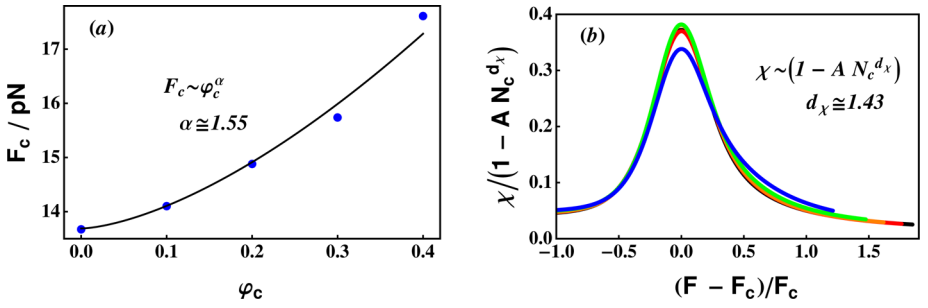

Figure 5. (a) Critical force (F_c) of the hairpin versus crowder volume fraction (φ_c). F_c displays a power law dependence on the volume fraction of crowding agent with an exponent (α) of 1.55. (b) Data collapse of the isothermal extensibility (χ) (Figure 4) shows that $\chi \approx (1 - AN_c^{d_\chi})X((F - F_c)/F_c)$, where the scaling function ($X(x)$) is independent of the number of crowders (N_c). Thus, the dependence of the isothermal extensibility on N_c is characterized by an exponent (d_χ) of 1.43. Black, red, orange, green, and blue curves, respectively, are for N_c = 0, 5000, 10000, 15000, and 20000.

folded state. The extent of structure formation can be inferred using the average fraction of native contacts, $\langle Q \rangle$. In Figure 6,

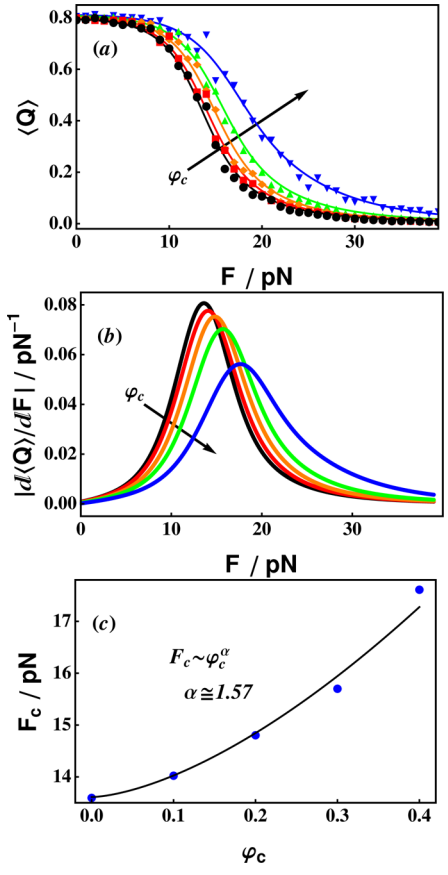

Figure 6. (a) Average fraction of native contacts ($\langle Q \rangle$) versus applied tension (F). (b) Absolute value of $d\langle Q \rangle/dF$ versus F. The force that maximizes $|d\langle Q \rangle/dF|$ at a particular volume fraction φ_c corresponds to the critical force $F_c(\varphi_c)$ at φ_c. (c) A plot of F_c versus φ_c verifies the results illustrated in Figure 5a; $F_c \approx \varphi_c^{\alpha}$ where $\alpha \cong 1.6$.

we show $\langle Q \rangle$ as a function of F. For all values of F, the crowding particles increase $\langle Q \rangle$, which is a reflection of the enhanced stabilization of the native state of β-hairpin at $\varphi_c \neq 0$. Let us define F_m using $\langle Q \rangle = 0.5$ at $\varphi_c = 0$. At this value of F_m, Figure 6a shows that $\langle Q \rangle \approx 0.75$ at $\varphi_c = 0.4$. The critical force, F_c, can identified with the force at which $|d\langle Q \rangle/dF|$ (Figure 6b) achieves a maximum. It is clear that F_c is an increasing function of φ_c (Figure 6c). Just as in Figure 4a, where F_c is identified with the maximum in the isothermal extensibility, we find that $F_c \approx \varphi_c^{\alpha}$ with $\alpha \approx 1.6$ (Figure 6c). The numerical simulations using different measures confirm the scaling predictions showing the power law increase in the φ_c-dependent critical force required to rupture the hairpin.

Osmotic (or Disjoining) Pressure Explains the Origin of φ_c-Dependent F_c. Insights into our results can be obtained by viewing the depletion forces from a different perspective. Because of the repulsive interaction between the crowders and the polypeptide chain, the crowding particles are depleted from the surface of the protein. In the process, the crowding particles not only gain translational entropy, but they also exert an osmotic pressure on the polypeptide chain, thus forcing it to adopt a compact structure. In other words, the crowders can be viewed as providing an isothermal and *isobaric* bath for the hairpin. In such a case, it is natural to assume that F_c is proportional to the average pressure (P) associated with a hard sphere fluid at that density and volume fraction:

$$F_c = mP + b \tag{16}$$

where m and b are constants to be determined.

The disjoining or osmotic pressure can, in turn, be calculated from the contact value $g(\sigma) \equiv \lim_{r \to \sigma^+} g(r)$ of the crowder−crowder radial distribution function using the standard relation,

$$P = \rho k_B T(1 + 4\varphi_c g(\sigma)) \tag{17}$$

Equation 17 follows from the virial-based expression for hard sphere systems,

$$\frac{P}{\rho k_B T} = 1 - \frac{2\pi\rho}{3k_B T} \int_0^{\infty} g(r) \frac{d\upsilon}{dr} r^3 \, dr \tag{18}$$

via the substitution $g(r) = \psi(r)\, e^{-\beta\upsilon(r)}$ and by noting that the Boltzmann factor $e^{-\beta\upsilon} = \theta(r - \sigma)$ for hard spheres where $\theta(x)$ is the step function.

From the Figure 7a showing the crowder−crowder $g(r)$ at volume fractions φ_c = 0.1, 0.2, 0.3, and 0.4, we computed $g(\sigma)$, which was subsequently used to determine the average pressure at each φ_c. The linear correlation coefficient (r) between the two variables (F and P) was determined to be 0.99657 (Figure 7b). The probability that five measurements of two uncorrelated random variables would yield a correlation coefficient this high is $2\Gamma(2)/[\sqrt{\pi}\Gamma(3/2)]\int_{0.99657}^{1}(1 - x^2)^{1/2} dx = 0.00024$, where $\Gamma(x)$ is Euler's gamma function. In Figure 7b, we provide the best fit line to the data yielding m = 0.24 nm^2 and b = 13.84 pN. Thus, F_c is linearly related to the osmotic pressure arising from depletion forces, whose strength is a measure of the stabilization of the ordered state.

dx.doi.org/10.1021/jp402922q | J. Phys. Chem. B 2013, 117, 13107−13114

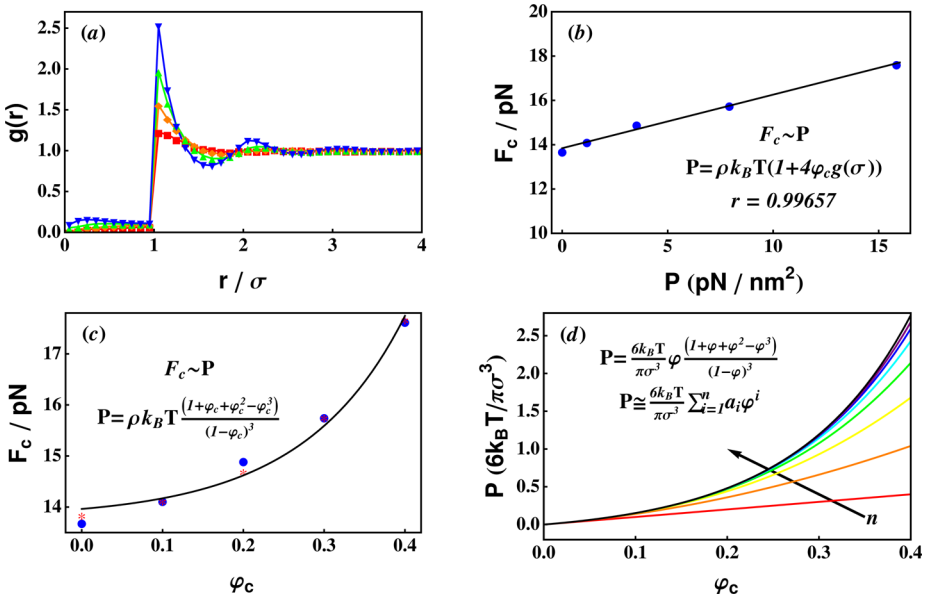

Figure 7. (a) Crowder−crowder radial distribution fucntion ($g(r)$) versus separation distance (r/σ). Red squares, orange diamonds, green up triangles, and blue down triangles, respectively, correspond to φ_c = 0.1, 0.2, 0.3, and 0.4. (b) The contact value $g(\sigma) \equiv \lim_{r\to\sigma^+} g(r)$ from (a) was used to calculate the average pressure (P) of the hard spheres at each φ_c using the virial derived equation $P = \rho k_B T(1 + 4\varphi_c g(\sigma))$. A plot of F_c versus P revealed a highly significant correlation with a linear correlation coefficient r = 0.99657. Blue circles correspond to measured data, and the black solid line corresponds to the best fit line $F_c = mP + b$, where m = 0.24 nm^2 and b = 13.84 pN. (c) The dependence of F_c on φ_c. Blue circles correspond to simulation data. The solid black curve corresponds to the best-fit line relating F_c to the pressure ($P(\varphi_c)$) at φ_c, where P was calculated from the semiempirical Carnahan−Starling equation of state: $P = \rho k_B T(1 + \varphi_c + \varphi_c^2 - \varphi_c^3)/(1 - \varphi_c)^3$. The red stars also correspond to a best-fit line relating F_c to $P(\varphi_c)$, where P was calculated as in panel b. (d) P versus φ_c as calculated via the Carnahan−Starling equation of state (black) and after truncating a Taylor-series expansion ($P \cong 6k_B T/(\pi\sigma^3 \sum_{i=1}^{n} a_i \varphi_c^i)$) of this equation of state about φ_c = 0 after n = 1 (red), 2 (orange), 3 (yellow), 4 (green), 5 (cyan), 6 (blue), and 7 (purple) terms.

In order to obtain the dependence of F_c on φ_c, a reliable relationship between P and φ_c needs to be established. Although P can be calculated using simulations, it would be convenient to obtain approximate analytically calculable estimates of P. The average pressure associated with the hard spheres can be determined at all φ_c using the successful semiempirical Carnahan−Starling equation of state:

$$\frac{P}{\rho k_B T} = \frac{1 + \varphi_c + \varphi_c^2 - \varphi_c^3}{(1 - \varphi_c)^3} \tag{19}$$

Figure 7c shows F_c versus φ_c (blue circles), as well as the curve associated with the best-fit linear relation between F_c and P calculated using eq 19. This linear relation yielded m = 0.17 nm^2 and b = 13.96 pN, which are close to the values obtained by fitting F_c to numerically computed values for P. The stars illustrate (φ_c,F_c) ordered pairs associated with the best-fit linear relation between F_c and P as calculated from eq 17 (as in Figure 7b). We surmise that P approximated by eq 19 can be used to obtain accurate estimates of F_c given knowledge of the coefficients m and b.

Finally, the accuracy of the Carnahan−Starling equation is assessed by plotting in Figure 7d eq 19 as well as several truncated Taylor-series expansions:

$$P \cong \frac{6k_B T}{\pi\sigma^3} \sum_{i=1}^{n} a_i \varphi_c^i \tag{20}$$

of this equation of state. Note that the relative error associated with the linear approximation (n = 1) of 0.342651 is large at φ_c = 0.1, while the relative error is only 0.0326804 at φ_c = 0.4 when n = 7 terms are included in the expansion. The coefficients of the expansions are a_1 = 1, a_2 = 4, a_3 = 10, a_4 = 18, a_5 = 28, a_6 = 40, and a_7 = 54. The linear relation between F_c and P shows that close to φ_c = 0, F_c should depend only linearly on φ_c because P is approximately linearly dependent on φ_c for small φ_c. However, in order to determine the value of F_c at an arbitrary φ_c, one should first determine the appropriate linear relation between F_c and P. The critical force F_c can then be determined at an arbitrary φ_c using the linear relation and approximate estimate of P given in eq 19.

CONCLUSIONS

Using simple theoretical arguments and extensive MC simulations of a three-dimensional off-lattice model, we have demonstrated for the first time that the critical force for unzipping a biopolymer under tension obeys a nonlinear dependence on the volume fraction of crowding agent. This dependence can be characterized by a power law dependence with an exponent $\alpha \cong 1.6$: $F_c \approx \varphi_c^{\alpha}$. The exponent α is surprisingly close to the scaling prediction $1/\nu$ with $\nu \approx 3/5$.

The numerical findings and scaling predictions can be understood by noting that the crowders provide an isobaric environment for the protein. The osmotic pressure arises from the depletion forces due to expulsion of the crowding particles from the protein and is entropic in origin. Because of the osmotic pressure, unzipping requires that the tension imposed on the hairpin perform mechanical work against the isotropic pressure. These arguments are fully confirmed in simulations, which demonstrate that F_c has a highly significant linear correlation with the pressure (P) of the hard-sphere crowding particles in which it is embedded. To determine F_c at an arbitrary φ_c, one should first determine the linear dependence of F_c on P. The exact relation connecting F_c to φ_c then follows

dx.doi.org/10.1021/jp402922q | J. Phys. Chem. B 2013, 117, 13107−13114

from the Carnahan−Starling equation of state. This relationship shows that F_c displays an approximately linear dependence on φ_c for volume fractions near $\varphi_c = 0$. However, when examined over a large range of φ_c, we expect that F_c should increase nonlinearly with φ_c as indicated by the scaling predictions exploiting the relationship between crowding and confinement.

Two comments about the scaling predictions are important to make. (i) The exponent α relating the increase in F_c to φ_c, although related to the Flory exponent (ν), is likely to depend both on the nature of the unfolded states of the protein and the shape of the crowding particles. If the overall shape of the unfolded state is nonspherical as is clearly the case for the hairpin (Figure 1) then $\alpha \approx 1.6$. On the other hand, if the unfolded state is spherical on average, as is likely to be the case for larger proteins, then it is likely $\alpha \approx 5/9$, as argued previously.[18] (ii) The theoretical predictions are based on a mean-field picture in which it is assumed that crowding (modeled with hard spheres) results in the protein being localized to a cavity. Thus, fluctuations in the crowding particles are ignored. These, especially close to the protein, could have significant effects. The good agreement between scaling predictions and simulations suggests that the fluctuation effects are not significant, at least for the case tested here. In principle, the importance of fluctuations can be tested by fixing the locations of the crowding particles. Such quenched simulations are equivalent to the present annealed simulations for the properties of the proteins because in a large sample containing fixed obstacles the protein would sample many distinct environments. This is then the same as performing annealed simulations. Therefore, we expect that the scaling properties predicted and tested here will not change even if the simulations are done by fixing the locations of the crowding particles. Additional simulations on proteins, rather than polypeptide chains forming secondary structures, would be needed to obtain accurate values of α.

There are only very few experiments probing the limits of mechanical stability of proteins in the presence of crowding agents. For example, atomic force microscopy has been used to investigate the effects of dextran on the mechanical stability of proteins.[52] These researchers found $F_c \approx \varphi_c$ for $\varphi_c \in [0.0,0.3]$ and nonlinearity only for $\varphi_c > 0.3$. It is important to note that their experimental setup is of an inherently nonequilibrium character; one end of a protein is extended at a constant speed, while the other end is used to probe the chain's tension. Furthermore, the protein examined (ubiquitin) is unlikely to be a two-state folder and may undergo distinct unzipping reactions at multiple tensions. In this case, the effects of crowding in an energy landscape with multiple barriers[65] may have to be studied. Because of the nonequilibrium nature of the AFM setup, it would be desirable to verify the predictions of the present work using laser optical tweezer experiments in which small constant forces can be applied.

AUTHOR INFORMATION

Corresponding Author

*E-mail address: thirum@umd.edu.

Notes

The authors declare no competing financial interest.

ACKNOWLEDGMENTS

We are grateful to the National Institutes of Health (Grant GM089685) for supporting the research. The authors kindly thank the National Energy Research Scientific Computing (NERSC) Center for significant computational time and resources.

REFERENCES

(1) Bryngelson, J. D.; Wolynes, P. G. Spin glasses and the statistical mechanics of protein folding. *Proc. Natl. Acad. Sci. U. S. A.* **1987**, *84*, 7524−7528.

(2) Bryngelson, J. D.; Wolynes, P. G. Intermediates and barrier crossing in a random energy model (with applications to protein folding). *J. Phys. Chem.* **1989**, *93*, 6902−6915.

(3) Bryngelson, J.; Onuchic, J.; Socci, N.; Wolynes, P. Funnels, Pathways, and the Energy Landscape of Protein-Folding - A Synthesis. *Proteins: Struct., Funct., Genet.* **1995**, *21*, 167−195.

(4) Camacho, C. J.; Thirumalai, D. Kinetics and Thermodynamics of Folding in Model Proteins. *Proc. Natl. Acad. Sci. U. S. A.* **1993**, *90*, 6369−6372.

(5) Hofmann, H.; et al. Polymer Scaling Laws of Unfolded and Intrinsically Disordered Proteins Quantified with Single-Molecule Spectroscopy. *Proc. Natl. Acad. Sci. U. S. A.* **2012**, *109*, 16155−16160.

(6) Wolynes, P. G.; Eaton, W. A.; Fersht, A. R. Chemical physics of protein folding. *Proc. Natl. Acad. Sci. U. S. A.* **2012**, *109*, 17770−17771.

(7) Thirumalai, D.; O'Brien, E. P.; Morrison, G.; Hyeon, C. Theoretical perspectives on protein folding. *Annu. Rev. Biophys.* **2010**, *39*, 159−183.

(8) Betancourt, M. R.; Thirumalai, D. Exploring the kinetic requirements for enhancement of protein folding rates in the GroEL cavity. *J. Mol. Biol.* **1999**, *287*, 627−644.

(9) Baumketner, A.; Jewett, A.; Shea, J. Effects of Confinement in Chaperonin Assisted Protein Folding: Rate Enhancement by Decreasing the Roughness of the Folding Energy Landscape. *J. Mol. Biol.* **2003**, *332*, 701−713.

(10) Jewett, A.; Baumketner, A.; Shea, J. Accelerated Folding in the Weak Hydrophobic Environment of a Chaperonin Cavity: Creation of an Alternate Fast Folding Pathway. *Proc. Natl. Acad. Sci. U. S. A.* **2004**, *101*, 13192−13197.

(11) Hyeon, C.; Lorimer, G. H.; Thirumalai, D. Dynamics of Allosteric Transition in GroEL. *Proc. Natl. Acad. Sci. U. S. A.* **2006**, *103*, 18939−18944.

(12) Hyeon, C.; Onuchic, J. N. Internal strain regulates the nucleotide binding site of the kinesin leading head. *Proc. Natl. Acad. Sci. U. S. A.* **2007**, *104*, 2175−2180.

(13) Hyeon, C.; Onuchic, J. N. Mechanical control of the directional stepping dynamics of the kinesin motor. *Proc. Natl. Acad. Sci. U. S. A.* **2007**, *104*, 17382−17387.

(14) Tehver, R.; Thirumalai, D. Rigor to Post-Rigor Transition in Myosin V: Link between the Dynamics and the Supporting Architecture. *Structure* **2010**, *18*, 471−481.

(15) Koga, N.; Takada, S. Folding-based molecular simulations reveal mechanisms of the rotary motor f1-atpase. *Proc. Natl. Acad. Sci. U. S. A.* **2006**, *103*, 5367−5372.

(16) Zhang, Z.; Thirumalai, D. Dissecting the Kinematics of the Kinesin Step. *Structure* **2012**, *20*, 628−640.

(17) Zhou, H. X.; Rivas, G.; Minton, A. P. Macromolecular crowding and confinement: Biochemical, biophysical, and potential physiological consequences. *Annu. Rev. Biophys.* **2008**, *37*, 375−397.

(18) Pincus, D.; Hyeon, C.; Thirumalai, D. Effects of Trimethylamine N-Oxide (TMAO) and Crowding Agents on the Stability of RNA Hairpins. *J. Am. Chem. Soc.* **2008**, *130*, 7364−7372.

(19) Denesyuk, N. A.; Thirumalai, D. Crowding Promotes the Switch from Hairpin to Pseudoknot Conformation in Human Telomerase RNA. *J. Am. Chem. Soc.* **2011**, *133*, 11858−11861.

(20) Kilburn, D.; Roh, J. H.; Guo, L.; Briber, R.; Woodson, S. A. Molecular Crowding Stabilizes Folded RNA Structure by the Excluded Volume Effect. *J. Am. Chem. Soc.* **2010**, *132*, 8690−8696.

(21) Minton, A. Excluded volume as a determinant of macromolecular structure and reactivity. *Biopolymers* **1981**, *20*, 2093−2120.

(22) Minton, A. P.; Wilf, J. Effect of macromolecular crowding upon the structure and function of an enzyme - glyceraldehyde-3-phosphate dehydrogenase. *Biochemistry* **1981**, *20*, 4821−4826.
(23) Thirumalai, D. Isolated polymer molecule in a random environment. *Phys. Rev. A: Gen. Phys.* **1988**, *37*, 269−276.
(24) Zimmerman, S. B.; Minton, A. P. Macromolecular crowding - biochemical, biophysical, and physiological consequences. *Annu. Rev. Biophys. Biomol. Struct.* **1993**, *22*, 27−65.
(25) Zimmerman, S. B.; Murphy, L. D. Macromolecular crowding and the mandatory condensation of DNA in bacteria. *FEBS Lett.* **1996**, *390*, 245−248.
(26) Kidoaki, S.; Yoshikawa, K. Folding and unfolding of a giant duplex-DNA in a mixed solution with polycations, polyanions and crowding neutral polymers. *Biophys. Chem.* **1999**, *76*, 133−143.
(27) Sasahara, K.; McPhie, P.; Minton, A. P. Effect of dextran on protein stability and conformation attributed to macromolecular crowding. *J. Mol. Biol.* **2003**, *326*, 1227−1237.
(28) Minton, A. P. Models for excluded volume interaction between an unfolded protein and rigid macromolecular cosolutes: Macromolecular crowding and protein stability revisited. *Biophys. J.* **2005**, *88*, 971−985.
(29) Cheung, M. S.; Klimov, D.; Thirumalai, D. Molecular crowding enhances native state stability and refolding rates of globular proteins. *Proc. Natl. Acad. Sci. U. S. A.* **2005**, *102*, 4753−4758.
(30) Cheung, M. S.; Thirumalai, D. Effects of crowding and confinement on the structures of the transition state ensemble in proteins. *J. Phys. Chem. B* **2007**, *111*, 8250−8257.
(31) Stagg, L.; Zhang, S. Q.; Cheung, M. S.; Wittung-Stafshede, P. Molecular crowding enhances native structure and stability of alpha/beta protein flavodoxin. *Proc. Natl. Acad. Sci. U. S. A.* **2007**, *104*, 18976−18981.
(32) Homouz, D.; Perham, M.; Samiotakis, A.; Cheung, M. S.; Wittung-Stafshede, P. Crowded, cell-like environment induces shape changes in aspherical protein. *Proc. Natl. Acad. Sci. U. S. A.* **2008**, *105*, 11754−11759.
(33) Mittal, J.; Best, R. Dependence of Protein Folding Stability and Dynamics on the Density and Composition of Macromolecular Crowders. *Biophys. J.* **2010**, *98*, 315−320.
(34) Asakura, S.; Oosawa, F. On interaction between two bodies immersed in a solution of macromolecules. *J. Chem. Phys.* **1954**, *22*, 1255−1256.
(35) Asakura, S.; Oosawa, F. Interaction between particles suspended in solutions of macromolecules. *J. Polym. Sci.* **1958**, *33*, 183−192.
(36) Vrij, A. Polymers at interfaces and interactions in colloidal dispersions. *Pure Appl. Chem.* **1976**, *48*, 471−483.
(37) Verma, R.; Crocker, J.; Lubensky, T.; Yodh, A. Entropic colloidal interactions in concentrated DNA solutions. *Phys. Rev. Lett.* **1998**, *81*, 4004−4007.
(38) Crothers, D. M.; Kallenbach, N. R.; Zimm, B. H. Melting transition of low-molecular-weight DNA - theory and experiment. *J. Mol. Biol.* **1965**, *11*, 802.
(39) Kittel, C. Phase transition of a molecular zipper. *Am. J. Phys.* **1969**, *37*, 917−920.
(40) Fixman, M.; Freire, J. J. Theory of DNA melting curves. *Biopolymers* **1977**, *16*, 2693−2704.
(41) Azbel, M. Y. DNA sequencing and helix-coil transition. 1. Theory of DNA melting. *Biopolymers* **1980**, *19*, 61−80.
(42) Anshelevich, V. V.; Vologodskii, A. V. The effect of sequence heterogeneity on DNA melting kinetics. *J. Biomol. Struct. Dyn.* **1986**, *4*, 251−262.
(43) Essevaz-Roulet, B.; Bockelmann, U.; Heslot, F. Mechanical separation of the complementary strands of DNA. *Proc. Natl. Acad. Sci. U. S. A.* **1997**, *94*, 11935−11940.
(44) Peyrard, M.; Bishop, A. R. Statistical mechanics of a nonlinear model for DNA denaturation. *Phys. Rev. Lett.* **1989**, *62*, 2755−2758.
(45) Bockelmann, U.; Essevaz-Roulet, B.; Heslot, F. DNA strand separation studied by single molecule force measurements. *Phys. Rev. E: Stat. Phys., Plasmas, Fluids, Relat. Interdiscip. Top.* **1998**, *58*, 2386−2394.
(46) Clausen-Schaumann, H.; Rief, M.; Tolksdorf, C.; Gaub, H. E. Mechanical stability of single DNA molecules. *Biophys. J.* **2000**, *78*, 1997−2007.
(47) Wu, P.; Sugimoto, N. Transition characteristics and thermodynamic analysis of DNA duplex formation: a quantitative consideration for the extent of duplex association. *Nucleic Acids Res.* **2000**, *28*, 4762−4768.
(48) Klimov, D. K.; Newfield, D.; Thirumalai, D. Simulations of β-hairpin folding confined to spherical pores using distributed computing. *Proc. Natl. Acad. Sci. U. S. A.* **2002**, *99*, 8019−8024.
(49) Hyeon, C.; Thirumalai, D. Mechanical unfolding of rna hairpins. *Proc. Natl. Acad. Sci. U. S. A.* **2005**, *102*, 6789−6794.
(50) Munoz, V.; Thompson, P.; Hofrichter, J.; Eaton, W. Folding Dynamics and Mechanism of Beta-Hairpin Formation. *Nature* **1997**, *390*, 196−199.
(51) Ping, G.; Yang, G.; Yuan, J. M. Depletion force from macromolecular crowding enhances mechanical stability of protein molecules. *Polymer* **2006**, *47*, 2564−2570.
(52) Yuan, J. M.; et al. The effects of macromolecular crowding on the mechanical stability of protein molecules. *Protein Sci.* **2008**, *17*, 2156−2166.
(53) Klimov, D. K.; Thirumalai, D. Mechanisms and kinetics of β-hairpin formation. *Proc. Natl. Acad. Sci. U. S. A.* **2000**, *97*, 2544−2549.
(54) Pande, V.; Rokhsar, D. Molecular Dynamics Simulations of Unfolding and Refolding of a Beta-Hairpin Fragment of Protein G. *Proc. Natl. Acad. Sci. U. S. A.* **1999**, *96*, 9062−9067.
(55) Dinner, A.; Lazaridis, T.; Karplus, M. Understanding Beta-Hairpin Formation. *Proc. Natl. Acad. Sci. U. S. A.* **1999**, *96*, 9068−9073.
(56) Bryant, Z.; Pande, V.; Rokhsar, D. Mechanical Unfolding of a Beta-Hairpin UsingMolecular Dynamics. *Biophys. J.* **2000**, *78*, 584−589.
(57) Zhou, R.; Berne, B.; Germain, R. The Free Energy Landscape for Beta Hairpin Folding in Explicit Water. *Proc. Natl. Acad. Sci. U. S. A.* **2001**, *98*, 14931−14936.
(58) Best, R. B.; Mittal, J. Microscopic Events in Beta-Hairpin Folding from Alternative Unfolded Ensembles. *Proc. Natl. Acad. Sci. U. S. A.* **2011**, *108*, 11087−11092.
(59) Bhattacharya, A.; Best, R. B.; Mittal, J. Smoothing of the GB1 Hairpin Folding Landscape by Interfacial Confinement. *Biophys. J.* **2012**, *103*, 596−600.
(60) Baumgärtner, A.; Binder, K. Monte Carlo studies on the freely jointed polymer chain with excluded volume interaction. *J. Chem. Phys.* **1979**, *71*, 2541−2545.
(61) Honeycutt, J.; Thirumalai, D. Static properties of polymer-chains in porous-media. *J. Chem. Phys.* **1989**, *90*, 4542−4559.
(62) Mittal, J.; Best, R. B. Thermodynamics and Kinetics of Protein Folding under Confinement. *Proc. Natl. Acad. Sci. U. S. A.* **2008**, *105*, 20233−20238.
(63) Wang, W.; Xu, W. X.; Levy, Y.; Trizac, E.; Wolynes, P. G. Confinement Effects on the Kinetics and Thermodynamics of Protein Dimerization. *Proc. Natl. Acad. Sci. U. S. A.* **2009**, *106*, 5517−5522.
(64) Shental-Bechor, D.; Levy, Y. Folding of glycosylated proteins under confinement. *J. Chem. Phys.* **2011**, *135*, No. 141104.
(65) Hyeon, C.; Thirumalai, D. Multiple Barriers in Forced Rupture of Protein Complexes. *J. Chem. Phys.* **2012**, *137*, No. η055103.
(66) Allen, M. P.; Tildesley, D. J. *Computer Simulation of Liquids*; Oxford University Press: New York, 1987.